Experimental studies on the impact of adsorbent particle size on the adsorption chiller performance

Manila, Reddy Madhuri; Srinivasan, Kandadai; Dutta, Pradip

DOI
10.1016/j.ijrefrig.2024.04.021

Publication date
2024

Document Version
Final published version

Published in
International Journal of Refrigeration

International Journal of Refrigeration 164 (2024) 154–166

Contents lists available at ScienceDirect

International Journal of Refrigeration

journal homepage: www.elsevier.com/locate/ijrefrig

Experimental studies on the impact of adsorbent particle size on the adsorption chiller performance

Études expérimentales sur l'impact de la taille des particules d'adsorbant sur les performances d'un refroidisseur à adsorption

Reddy Madhuri Manila [a,d], Kandadai Srinivasan [b,c], Pradip Dutta [b,*]

[a] *Department of Mechanical Engineering, Indian Institute of Science, Bangalore, 560012, India*
[b] *Interdisciplinary Centre for Energy Research, Indian Institute of Science, Bangalore 560012, India*
[c] *Also with School of Engineering, University of Western Australia, Crawley WA 6009, Australia*
[d] *Currently at Process & Energy Department of the faculty of Mechanical Engineering, TU Delft, CB Delft 2628, the Netherlands*

ARTICLE INFO

Keywords:
Silica gel + water adsorption cooling
Particle size
Thermal diffusivity
Coefficient of performance
Cooling capacity

Mots clés:
Refroidissement par adsorption
Taille de particule
Diffusivité thermique
Coefficient de performance
Puissance frigorifique

ABSTRACT

Adsorption chiller dynamics and its effect on the performance are greatly influenced by the adsorbent particle size because they govern both the micro (intra-particle) and macro (inter-particle) heat and mass transfer resistances within the adsorber bed. The net effect of adsorbent particle size and shape on the overall cooling system performance is addressed here. Initial CFD analysis of columnar adsorber bed with silica gel + water as the working pair, assuming uniform spherical adsorbent, showed increased uptake capacity with smaller sized (0.23 mm radius) particles over bigger sized (0.8 mm radius) ones despite smaller vapor penetration depth of the former. Subsequently, the effect of adsorbent particle size and shape on the overall cooling system performance is investigated experimentally in a single-stage one-bed mode for RD 2060 (0.8 mm radius) and RD 3070 (0.23 mm radius) silica gel specimens. Though the smaller size of RD 3070 is favourable for the adsorption kinetics at the particle level, its non-spherical shape and highly non-uniform size distribution resulted in significantly lower permeability and thermal diffusivity of the packed adsorber bed, thus hindering the cyclic steady state throughput. For the same operating conditions, RD 2060 and RD 3070 yield a cooling capacity (CC) of 107 W and 22 W, respectively. Further, the coefficient of performance (COP) drops by 73% in the case of RD 3070. The present study indicates that the adsorber bed design must consider both the adsorbent size and shape, in addition to other system operational parameters to enhance performance indicators.

1. Introduction

Adsorption cooling systems are construed to be complementary to conventional vapor compression refrigeration systems due to their ability to operate with low enthalpy industrial waste heat or low-grade solar/geothermal energy for vapor compression. Thermal compression systems have been the subject of extensive research over the past few decades. Despite a well-developed knowledge base on these systems, their widespread implementation is impeded by low levels of performance metrics, such as the cooling capacity (CC) and coefficient of performance (COP).

A schematic of a typical adsorption cooling system is shown in Fig. 1. The principal components of an adsorption cooling system are evaporator, adsorber bed (thermal compressor), condenser, and an expansion device. Each refrigeration cycle involves three processes namely: evaporation, thermal compression (adsorption and desorption), and condensation.

The refrigerant evaporates at the evaporator temperature and the low-pressure refrigerant enters the adsorber bed where it undergoes thermal compression till the required pressure lift is achieved. The thermal compression itself comprises a series of four processes: i) adsorption, ii) preheating, iii) desorption, and iv) precooling.

i) Adsorption: The refrigerant at evaporator pressure enters the adsorber bed through the inlet and is adsorbed by the adsorbent.

* Corresponding author.
E-mail address: pradip@iisc.ac.in (P. Dutta).

https://doi.org/10.1016/j.ijrefrig.2024.04.021
Received 23 December 2023; Received in revised form 14 April 2024; Accepted 21 April 2024
Available online 22 April 2024

Nomenclature

A:	area [m^2]
d:	diameter of the particle [mm]
D_{eff}:	effective mass diffusivity [$m^2\ s^{-1}$]
g:	acceleration due to gravity [$m\ s^{-2}$]
h:	height of the water column [mm]
h_{ads}:	heat of adsorption [kJ kg^{-1}]
K:	permeability [m^2]
$\dot{m}$:	mass flow rate [$kg\ s^{-1}$]
p:	pressure [kPa]
R:	radius of the particle [mm]
T:	temperature [K]
u:	Darcy velocity [ms^{-1}]
V:	volume [mm^3]
X:	domain width representing thermal diffusion length scale [mm]
Y:	domain width representing vapor flow length scale [mm]

Greek symbols

ρ:	density (kg m^{-3})
ε:	porosity
φ:	uptake [kg kg^{-1}]
μ:	dynamic viscosity [Pa s]
λ:	thermal conductivity [W $m^{-1}\ K^{-1}$]

Subscripts

a:	air
ads:	adsorption
bed:	adsorber bed
cold:	cold water
cr:	critical value
e:	equilibrium
evap:	evaporator
p:	particle
w:	water

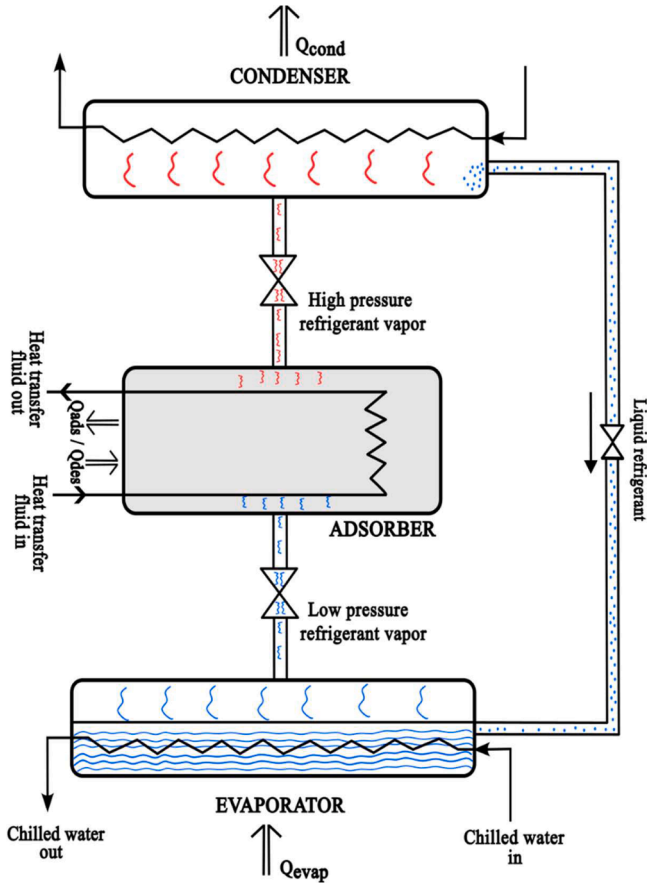

Fig. 1. Schematic of adsorption cooling system.

The heat of adsorption is carried away by the cold fluid circulating in the heat exchanger tubes.

ii) Preheating: During preheating, the adsorber bed is isolated by closing the inflow/outflow valves for the refrigerant flow, and the heat transfer fluid is switched to hot fluid for regenerating the adsorbed refrigerant. This heats the adsorber bed and the refrigerant starts desorbing. Since the desorption occurs at a constant volume, it results in the build-up of pressure within the adsorber bed.

iii) Desorption: The bed outlet valve is opened and the refrigerant at higher pressure is released to the condenser. The hot fluid is continuously circulated throughout this process to expel maximum amount of adsorbed refrigerant.

iv) Precooling: The adsorber bed is brought back to its initial state (bed pressure slightly less than the evaporator pressure) by isolating the adsorber bed and switching the heat transfer fluid to cold fluid.

The thermal compression cycle in an adsorber bed is depicted in Fig. 2 without the expansion device. As the thermal compression cycle is intermittent, employing a series of adsorber beds operating with a phase shift will yield a continuous throughput. The high-pressure refrigerant desorbed to the condenser undergoes phase change in the condenser and the liquid refrigerant is circulated back to the evaporator through an expansion device.

The performance of adsorption cooling systems operating with a specific refrigerant depends on the size and shape of adsorbent particles, adsorber bed design, and other operational parameters. Appropriate choice of adsorbent particle size can greatly enhance the cooling system performance as it has a direct impact on both heat and mass transfer dynamics within the adsorber bed. Chang et al. (Sen Chang et al., 2005) experimentally investigated the effect of silica gel particle size and thickness of the assembly on the heat and mass transfer characteristics of the adsorber bed. It was observed that thinner layers of larger-diameter adsorbent particles yield a better mass transfer performance of the system. The effect of boundary conditions and size of Fuji RD silica grains in monolayer configuration on the water sorption dynamics was studied experimentally by Glaznev and Aristov (Glaznev and Aristov, 2010). Subsequently, Aristov et al. (Aristov et al., 2012) experimentally analyzed the effect of adsorbent layer thickness on the water adsorption kinetics by varying the Fuji RD silica gel grain size from 0.2 to 1.8 mm. The key outcome of their studies was that there exists a "grain size insensitive" regime for small grains ($d < 0.5$ to 0.8 mm), while for $d \geq$ 0.8 mm, "grain size sensitive" regime is realized. This was followed by numerical studies (Aristov, 2013) of the adsorber heat exchanger with loose grain configuration using Fickian diffusion model for predicting the adsorption kinetics. Their qualitative conclusion was that the adsorbent grains must be small enough for realization of "lumped" mode, and large enough to avoid excessive pressure drop in the bed. Vodianitskaia et al. (Vodianitskaia et al., 2017) reported a comparative analysis of silica gel + water adsorption chiller where a single finned

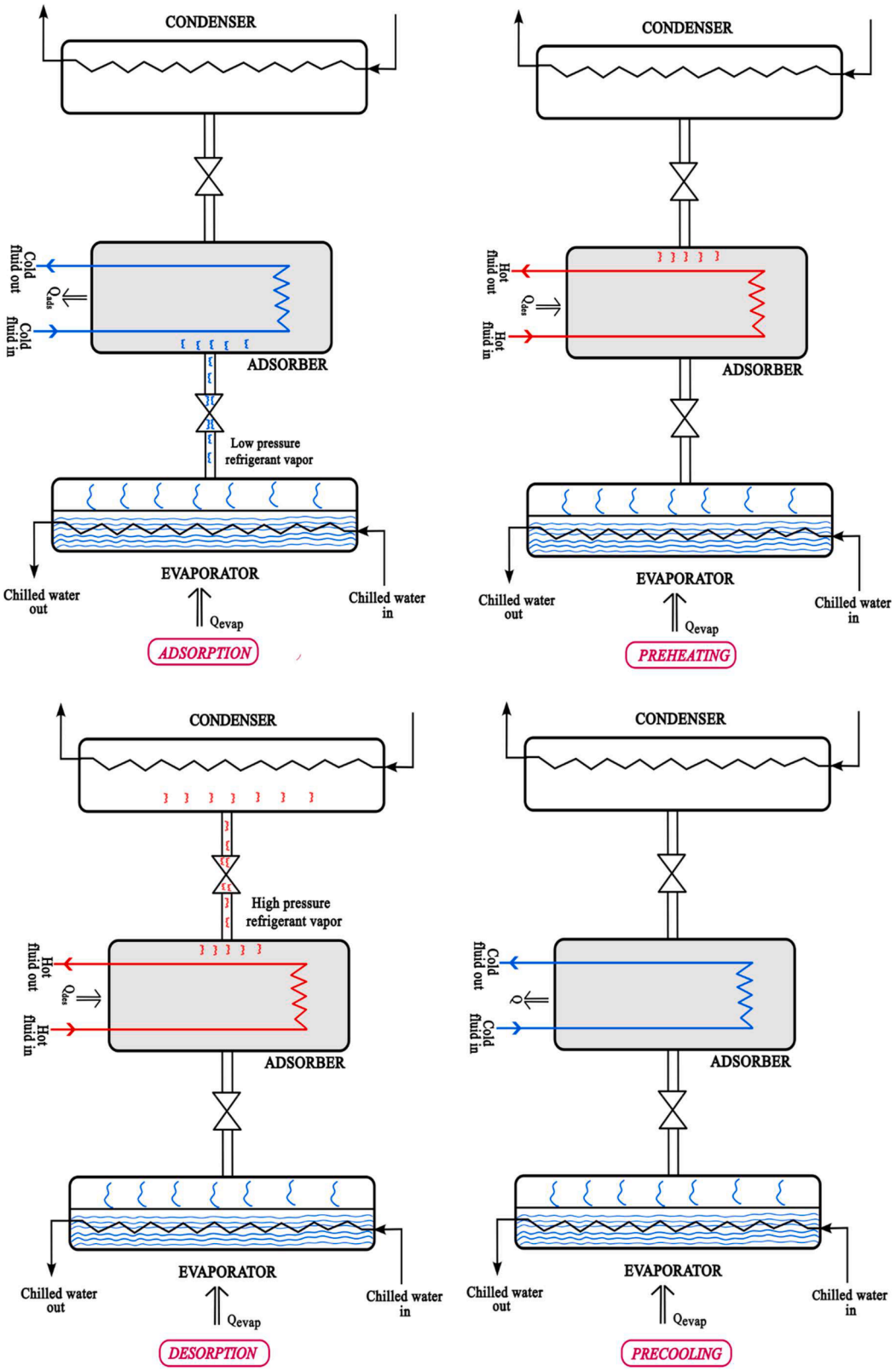

Fig. 2. Thermal compression cycle.

tube adsorber with a water-cooled condenser was used. Two particle sizes of 2.0 mm and 0.26 mm were investigated in loose grain configuration. Their conclusion was that the COP was 4% worse for the latter.

Niazmand et al. (Niazmand et al., 2013) performed numerical studies on a plate finned tube heat exchanger with SWS-1 L ($CaCl_2$ in mesoporous silica gel) as adsorbent. They found that an optimum performance for all conditions studied was obtained for the particle sizes in the range of 0.2–0.3 mm. Chakraborty et al. (Chakraborty et al., 2014) numerically studied the effect of grain size and number of layers on the performance of the silica gel and water adsorption chiller. They found

that smaller grain size and layers are preferable for better cooling capacity and COP. Mitra et al. (Mitra et al., 2018), from their two-dimensional simulation studies of tube-fin adsorber configuration for ethanol adsorption onto activated carbon, concluded that for smaller particle sizes, adsorption dynamics is a strong function of flow resistance of porous media. Three-dimensional simulation studies by Manila et al. (2020) on shell and tube type heat exchanger adsorber bed with RD silica gel as adsorbent confirmed the existence of a critical penetration depth for vapor flow and determined the optimum particle diameter with respect to uptake as 0.8 mm for the bed configuration studied.

Mahdavikhah et al. (Mahdavikhah et al., 2019) in their numerical study introduced a dimensionless parameter to determine appropriate bed pressure assumption approach in adsorber bed modelling. From their studies they found that at lower pressures, the inter-particle mass transfer resistance plays a major role for adsorbent particle diameters smaller than 0.25 mm and cannot be neglected. At higher working pressures this is applicable to larger sized adsorbent particles also. Akisawa et al. (AKISAWA et al., 2022) through their simulation studies demonstrated that performance superior to the single effect absorption cycle can be achieved with double effect adsorption cycle by appropriate allocation of adsorbent mass and cycle times.

From the foregoing discussion, it is evident that a majority of the studies in literature dedicated in investigating the effect of adsorbent particle size on the cooling system performance as a whole are numerical. A few experimental studies, however, pertain to loose-grain configuration with small number of layers. Practical adsorption refrigeration systems, on the other hand, generally involve large dimensions with multiple layers of packing of adsorbent. It is imminent that particle size effect needs to be evaluated under realistic conditions. The novelty of the present study lies in experimentally investigating the effect of adsorbent size and shape distribution in a packed adsorber bed at system level.

The primary objective of this paper is to bring out the effect of particle size and shape on the overall performance of an air-cooled silica gel + water adsorption refrigeration system with columnar adsorber beds. To this end, it is proposed to present the results obtained from single-stage one-bed mode of operation of thermal compressors. In the first mode, the adsorber was packed with 0.8 mm radius silica gel particles (RD 2060), which was followed by replacing the bed with the same amount of nominal 0.23 mm radius silica gel particles (RD 3070).

2. Characterization of silica gel specimen

The thermo-physical properties provided by the manufacturer (Fuji Silysia Chemical Ltd., Japan) for RD 2060 and 3070 are listed in Table 1 and Fig. 3 shows the pore size distribution for RD 2060. Both RD 2060 and RD 3070 possess the same pore size distribution (information provided by the manufacturer) and they vary only in the particle size distribution. In addition to thermo-physical properties, it is essential to determine the permeability of the packed adsorber bed as the inter-particle vapor diffusion inside an adsorber bed is a strong function of this property, which itself depends on the average particle size. The succeeding sub-sections focus on the determination of average particle size and permeability measurements.

Table 1
Thermophysical properties of silica gel specimens.

Parameter	RD 2060	RD 3070
Average particle diameter (mm)	1.60	0.21–0.60
Total surface area ($m^2\ g^{-1}$)	620	760
Pore-volume ($cm^3\ g^{-1}$)	0.37	0.42
Average pore diameter (nm)	2.30	2.20
Particle bulk density ($kg\ m^{-3}$)	1158	1170
Thermal conductivity ($W\ m^{-1}\ K^{-1}$)	0.20	0.14
Specific heat capacity ($kJ\ kg^{-1}\ K^{-1}$)	0.92	0.71

2.1. Particle size distribution

The optical microscopy analysis of the silica gel particles using Lieca M205 A is shown in Fig. 4.

The RD 2060 specimen is uniform and spherical (Fig. 4a)) with an average particle diameter of 1.6 mm (Table 1). But the RD 3070 specimen is non-spherical and irregular in size and shape (Fig. 4b)) with a size distribution (97.6%) ranging from 0.21 to 0.60 mm. In view of the wide distribution in size and shape, 110 optical microscope images of random samples of RD 3070 specimen are acquired. The images are then processed using the image processing software ImageJ. Firstly, the background is subtracted, and the threshold is set to eliminate particles less than 0.21 mm. Then, the particles are traced manually, and the area of each particle is determined. From the area, the equivalent radius is calculated. The probability density function of equivalent radius in Fig. 5 illustrates that most of the particles are of about 0.23 mm radius. The microporous structure of both specimens can be seen in Fig. 6. It is apparent that at the particle level, the RD 3070 specimen seems to possess more micropores than the RD 2060 which is also confirmed in Table 1.

2.2. Permeability measurement

Adsorption kinetics is one of the fundamental quantities which determine the adsorption potential of any given adsorbent + adsorbate pair. The linear driving force (LDF) model is widely used for predicting the adsorption kinetics. (Sircar and Hufton, 2000) For the present modeling of silica gel + water pair it is used in the following form:

$$\frac{\partial \varphi}{\partial t} = \frac{15 D_{eff}}{R^2}\ (\varphi_e - \varphi) \tag{1}$$

where effective diffusivity (D_{eff}) for RD silica gel is $2.54\times10^{-4}\ m^2\ s^{-1}$ (El-Sharkawy, 2011).

Although at the particle level, RD 3070 appears to have better adsorption characteristics than RD 2060, its performance will be governed by the porosity and permeability of the packed bed.

Permeability, which can be inferred as the ease with which a fluid can flow through a porous medium, is a measure of the flow conductance of the matrix. For flow through porous media, in Darcy's regime (low Reynolds number), the permeability is given by:

$$K = \frac{-\mu u}{\left(\frac{dp}{dx}\right)} \tag{2}$$

In a packed bed made of uniformly sized spheres (unconsolidated media) of mean particle diameter (d), this property can be predicted reasonably well from the widely used Carman-Kozeny equation (Kaviany, 1999):

$$K = \frac{\varepsilon^3 d^2}{180(1-\varepsilon)^2} \tag{3}$$

However, for non-spherical and non-uniform-sized particles/powders (consolidated media), the Kozeny theory does not hold (Carman, 1956). Using Eq. (3) for estimating the permeability of a bed packed with non-spherical particles will yield incorrect values. Consequently, these measurements were made in a simple laboratory setup described in Fig. 7. The test section consists of an acrylic chamber of height 400 mm with an inner diameter of 48 mm in which the RD silica gel specimen of known mass is filled. A 0.1 mm circular mesh is inserted both at the top and bottom to avoid any carryover of silica gel particles during the experiment. The T- sections at the top and bottom of the cylinder enable connecting a U-tube manometer on one side with provision for the entry and exit of compressed air on the other side. Distilled water is used as the manometric fluid. Compressed air of known mass flow rate enters the test chamber from the top of the cylinder and exits from the

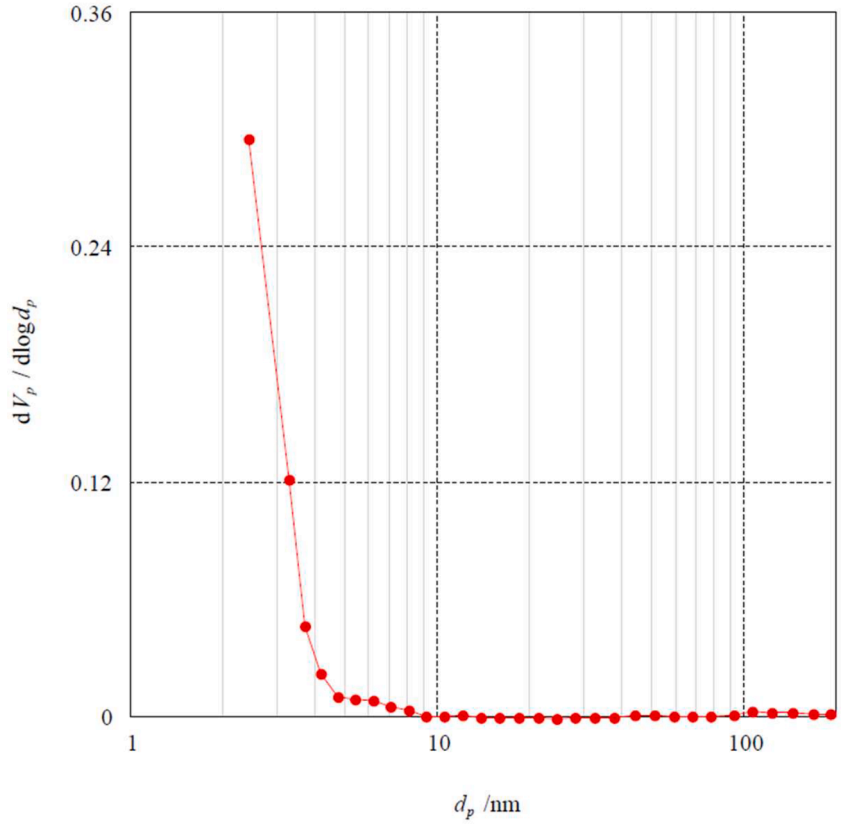

Fig. 3. Pore size distribution for RD 2060 silica gel.

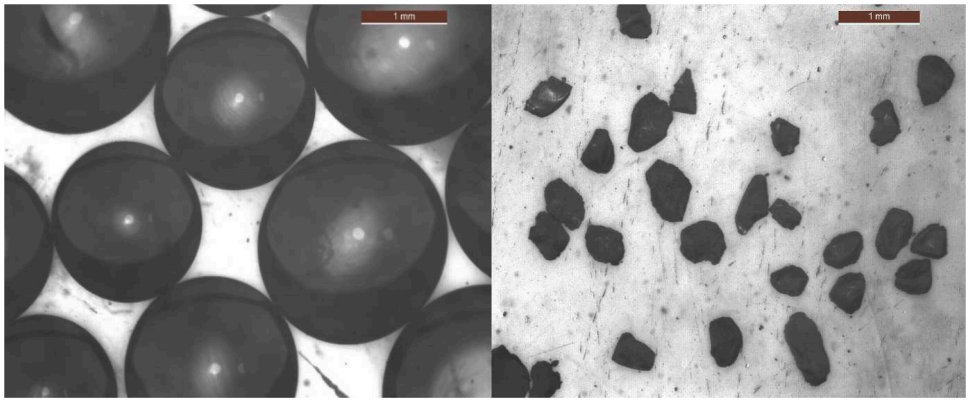

Fig. 4. Optical microscope image of: a) RD 2060 b) RD 3070 silica gel.

bottom to the ambient. The pressure drop is measured with a U-tube manometer for various mass flow rates. The mass flow rates are chosen such that they are within the same range as that encountered by a real adsorber bed during the adsorption process.

Eq. (2) can be re-written in terms of mass flow rate of air as follows:

$$K = \frac{-\mu\,\dot{m}}{\left(\frac{dp}{dx}\right)\rho_a A} \tag{4}$$

The permeability is then calculated by inserting the known values of μ, $\dot{m}$, ρ_a, cross-sectional area of flow (A) and pressure difference (dp) measured as ($\rho_w.g.h$).

The permeability measurements are initially performed for RD 2060. From the mass of the silica gel filled, bed dimensions, and density of silica gel, the randomly packed bed porosity is found to be 0.32. The permeability is then estimated from Eq. (3) and Eq. (4). Fig. 8 shows the comparison between experimental and empirical values of permeability for both specimens and the difference between the values is found to be within 3–5% for RD 2060. This reaffirms that the Carman-Kozeny equation (Eq. (3)) predicts the permeability accurately for uniform spheres. It also validates the technique adopted for permeability measurement.

The next set of measurements with RD 3070 yielded a bed porosity of 0.23 owing to its powder like texture because of higher interparticle interaction resistance and higher density. For the RD 3070 sample, there exists a considerable difference in the permeability values measured experimentally and determined empirically, which is evident from Fig. 8. Despite low porosity, the experimental permeability measured is

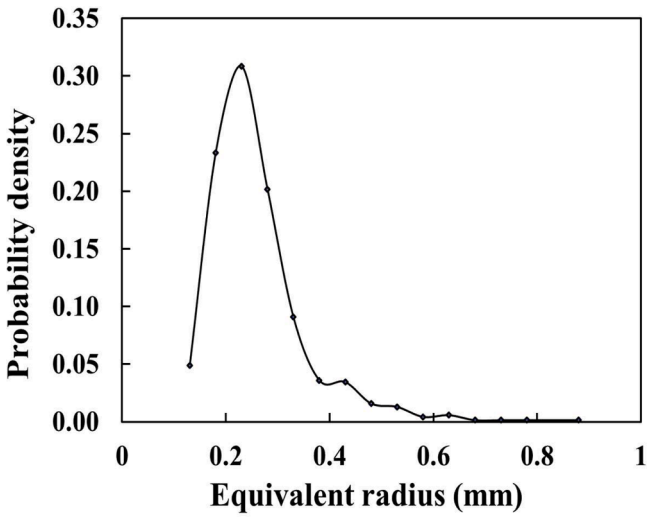

Fig. 5. Probability density of the equivalent radius of the RD 3070 sample.

one order higher than that calculated from Eq. (3) for spherical particles of an equivalent radius of 0.23 mm. This can be attributed to the existence of huge non-uniformity in the particle size and shape for a consolidated porous media (Kaviany, 1999). Since the measurements are carried out over limited time scale and geometry, it might result in the actual adsorber bed possessing a different porosity and hence a modified permeability. Also, the adsorbent particle loading, and repeated pressure cycling can cause these values to differ spatially as well. This phenomenon is more pronounced in the case of RD 3070 which has a highly random distribution of particle size and shape as seen in Fig. 4b).

3. Simulation studies

Prima facie, from Table 1, 0.23 mm size particles appear to have a larger surface area and micropore volume than 0.8 mm size specimen at the particle level. Intuitively, the former is expected to have better adsorption characteristics than the latter. This is also fortified by CFD studies of the adsorber bed presented in (Manila et al., 2020) based on the following assumptions:

i) adsorbent particles are spherical and uniform in size and shape.
ii) bed porosity remains the same irrespective of particle size.
iii) thermo-physical properties of adsorbent particles are independent of size.
iv) Carman-Kozeny relation is valid for permeability calculation for spherical particles.

It was shown that an optimum adsorbent particle radius in terms of uptake is 0.4 mm. That study also implied that adsorbent particles of 0.2 – 0.3 mm radius also show better uptake capacity than the 0.8 mm radius particle. Consequently, RD 3070 was taken up for further studies *vis-à-vis* RD 2060.

A *priori*, two-dimensional parametric CFD study for particle radii of 0.23 mm and 0.8 mm is carried out using COMSOL Multiphysics V5.6a and the modelling assumptions made in earlier work (Manila et al., 2020) discussed above are used in the present study as well. Three cases are considered which are as follows:

i) RD 2060 with permeability value calculated from Carman-Kozeny relation.
ii) RD 3070 with permeability calculated from Carman-Kozeny relation.
iii) RD 3070 with measured value of permeability as listed in Table 2 below.

The thermo-physical properties provided by the manufacturer are used for case i and one of the assumptions in modelling is that the thermo-physical properties of case ii remain same as that of case i. Bed porosity of 0.3 is chosen for cases i and ii assuming a packing density of 70% for spheres in a columnar bed. Whereas, to determine bed porosity in case iii, a known mass of adsorbent (RD 3070) is filled in a small columnar chamber with known dimensions (length and diameter). Then the solid fraction is calculated which in turn gives the bed porosity. This process is repeated multiple times to ensure repeatability. In all the three cases, the thermal diffusivity is calculated from the known values of bed density, thermal conductivity, and heat capacity.

A two-dimensional axisymmetric model considered for the CFD study is an adsorber bed of 10 mm radius and 560 mm length with an annular vapor space of 5 mm, as shown in Fig. 9. The initial temperature of the adsorber bed is set to 323 K. Isothermal cold wall condition of 303 K is imposed on the heat transfer fluid tube wall. Other boundaries are assumed to be adiabatic. The thermal non-equilibrium between the adsorber bed and the cold wall initiates the adsorption process. Vapor at evaporator pressure (p_{evap}) of 1.4 kPa enters from the inlet at the top which traverses axially as well as radially through the annular vapor passage during adsorption. This ensures that the vapor is available all along the length of the domain. The initial and boundary conditions for all the cases studied remain the same.

The adsorption kinetics is modelled using the LDF model given in Eq. (1). Fig. 10 shows the uptake variation during adsorption over 2250 s. It is evident that since the RD 3070 particles are assumed to be spherical (case ii above) and have the same thermophysical properties as that of RD 2060, they exhibit better uptake capacity than RD 2060. In addition, this case exhibits a faster adsorption rate at the start of adsorption process as the intra-particle mass diffusion resistance is less for smaller-sized particles. However, when the actual available thermo-physical

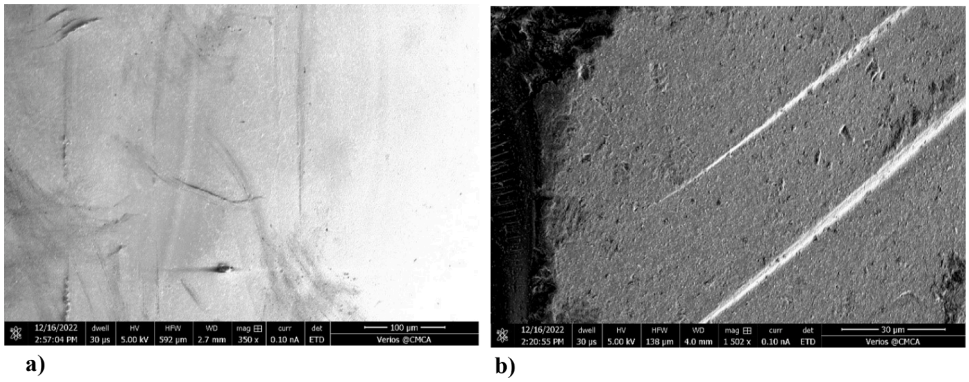

a) b)

Fig. 6. SEM images a) RD 2060 with a magnification factor of 16 and b) RD 3070 mm with a magnification factor of 13.

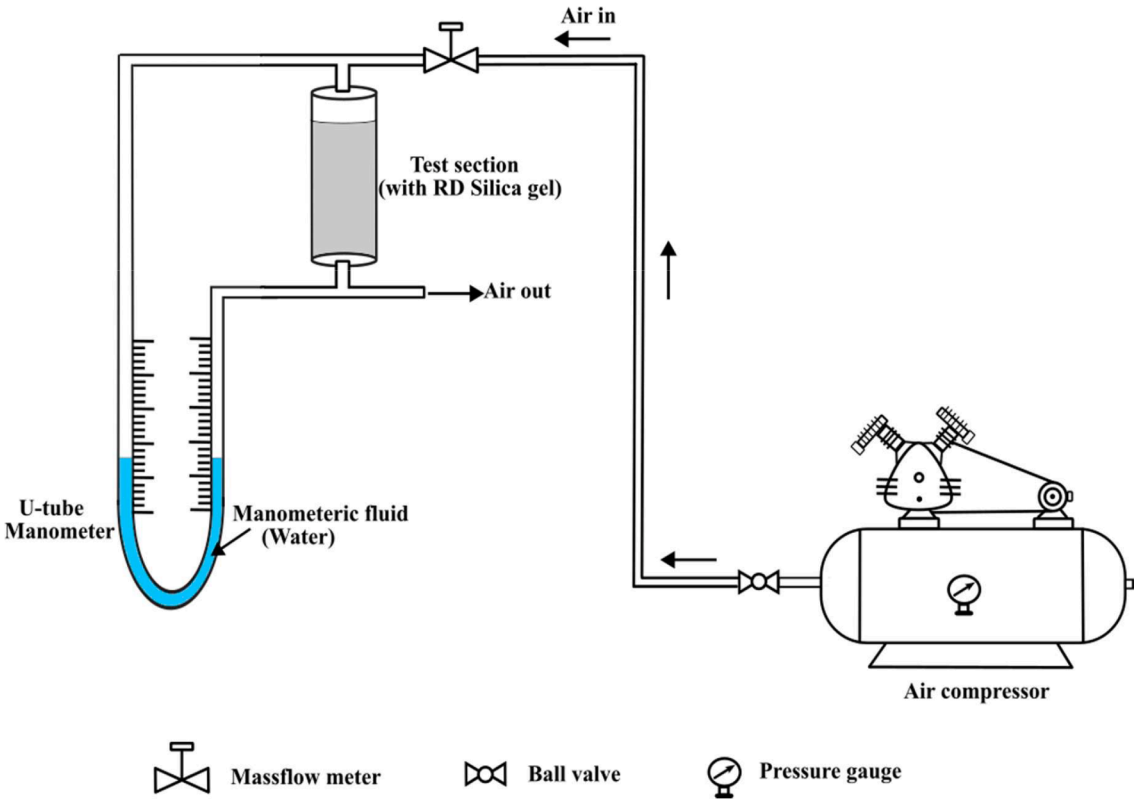

Fig. 7. Schematic of permeability measurement test set-up.

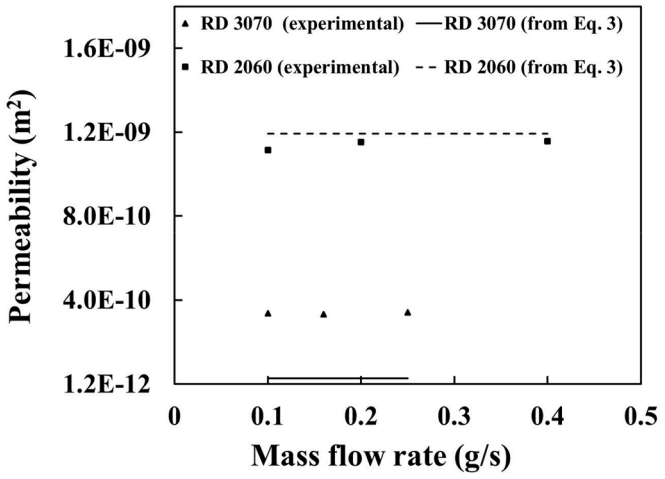

Fig. 8. Comparison of experimentally and empirically estimated values of permeability for RD 3070 and RD 2060.

properties are used with (case iii) – where the measured porosity (0.15) is 50% less than the assumed porosity (0.3) as in the other two cases, the uptake capacity of RD 3070 drastically decreases along with the rate of uptake despite the measured permeability being higher than its theoretical value.

4. Two-bed adsorption chiller experimental setup

A schematic of a single-stage, two-bed, air-cooled adsorption chiller with silica gel and water vapor as the working pair is shown in Fig. 11. The cooling load of the evaporator is from a constant temperature bath (JULABO FP80-SP). The deionized water in the evaporator flashes to steam at a low evaporator pressure of 1.7 kPa. The low-pressure vapor

Table 2
Data used in simulation.

Parameter	Value		
	RD 2060 (case i)	RD 3070 (case ii)	RD 3070 (case iii)
Radius (mm)	0.8	0.23	0.23* (equivalent)
Bed packing density (kg m^{-3})	822	822	1000*
Bed porosity	0.3	0.3	0.15*
Permeability (m^2)	8.2×10^{-10}	5.9×10^{-11}	3.39×10^{-11}* (6.59×10^{-12})^
Thermal diffusivity (m^2 s^{-1})	2.7×10^{-7}	2.7×10^{-7}	1.9×10^{-7}

*Measured data.
^From Carman-Kozeny relation, with modified porosity.

enters the adsorber bed, where it is thermally compressed to the condenser pressure of about 5.7 kPa.

The adsorber bed is essentially a shell and tube heat exchanger with a shell diameter of 160 mm and a length of 600 mm. The silica gel is packed on the shell side. A stainless-steel mesh (100 μm for RD 3070 and 500 μm for RD 2060) encloses and holds 5.6 kg of either specimen. It also provides an annular passage of 5 mm for vapor flow between the inner wall of the bed and the mesh. This facilitates the vapor to traverse both axially and radially decreasing the overall mass transfer resistance for adsorption. Each adsorber is provided with an ullage volume to dampen any pressure fluctuations, which will be different for each specimen, that may occur during steam valve operation. The heat of adsorption/regeneration is carried/supplied by the heat transfer fluid (cold/hot water) circulating in the heat exchanger tubes alternately regulated by a three-way water valve as shown in Fig. 11. Cold water at ambient temperature (at about 36 °C) is supplied during the cooling phase from a 150 L tank and the heat of adsorption is rejected in a dry cooler which is a finned-tube heat exchanger. A 75 L water tank with

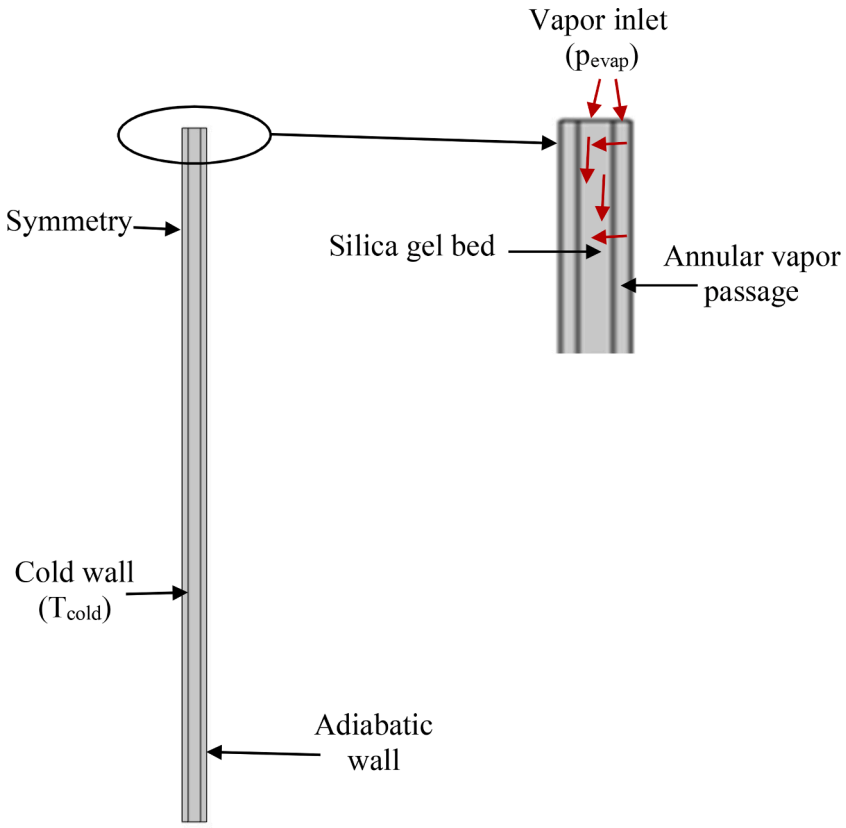

Fig. 9. 2D domain representing adsorber bed. Red coloured arrows represent the vapor flow direction.

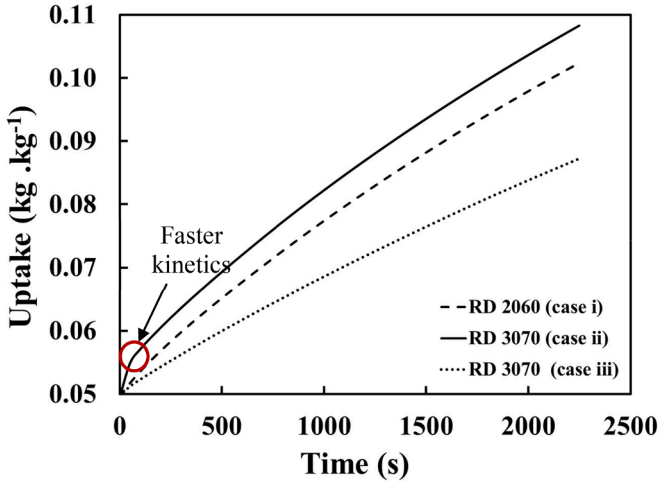

Fig. 10. Effect of particle size and shape on uptake capacity.

three electrical heaters (2 kW each) simulates the solar/waste heat and supplies the hot water (at about 85 °C) for regeneration. Motorized flow control valves on the return line of water circuits regulate the flow rates to a preset values which are 33 LPM for cold water and 25 LPM for hot water. The top flange of the adsorber bed houses two steam ports, one for the entry and another for the exit of steam, an absolute pressure sensor, and two thermowells for inserting the thermocouples at depths of 330 mm and 220 mm into the bed.

Since the adsorption chiller is air-cooled with the heat of condensation being rejected to the ambient, the thermal compression is carried out till the pressure in the adsorber bed rises to a value slightly higher than the saturation pressure corresponding to the condenser temperature. After attaining the required pressure lift, the high-pressure steam is desorbed to the condenser via plenum. The sytem is operated in open cycle wherein the condensate is collected in a calibrated tank located below the condenser.

T-type thermocouples with an accuracy of ±0.2 °C (TC Ltd.) and absolute pressure sensors (YOKOGAWA FP201A - K31) with a range of 0.1–50 kPa and uncertainty of ±0.05 kPa are used for the temperature and pressure measurements, respectively. Flow sensors of 0–100 LPM capacity situated at the outlet of the adsorber beds measure the hot/cold water flow rates. National Instruments (NI) PXIe controller is used for data acquisition (DAQ) and control. The system start-up and its steady-state operation are automated. The entire system must be evacuated before starting the experiments.

The above experimental set up can be operated either in single- or two-bed mode by closing their respective vapor valves. The first set of experiments were conducted with RD 2060 followed by regeneration at 85 °C under vacuum and replacing the adsorbent with RD 3070. The thermal compression cycle parameters (evaporator pressure, half cycle time, switching time and heat source temperature) chosen for RD 2060 were also used for RD 3070 in order to compare the performance of both the specimens.

5. Results and discussion

In this section, a discussion on the critical vapor penetration depth for RD 2060 and RD 3070 based on simulation studies is presented followed by the findings from experiments.

5.1. *Effect of critical vapor penetration depth from simulation studies*

In adsorbers with temperature swing adsorption, the critical vapor penetration depth (Y_{cr}) is defined as the vapor flow length from the inlet of the adsorber bed up to which the pressure drop is not significant. This

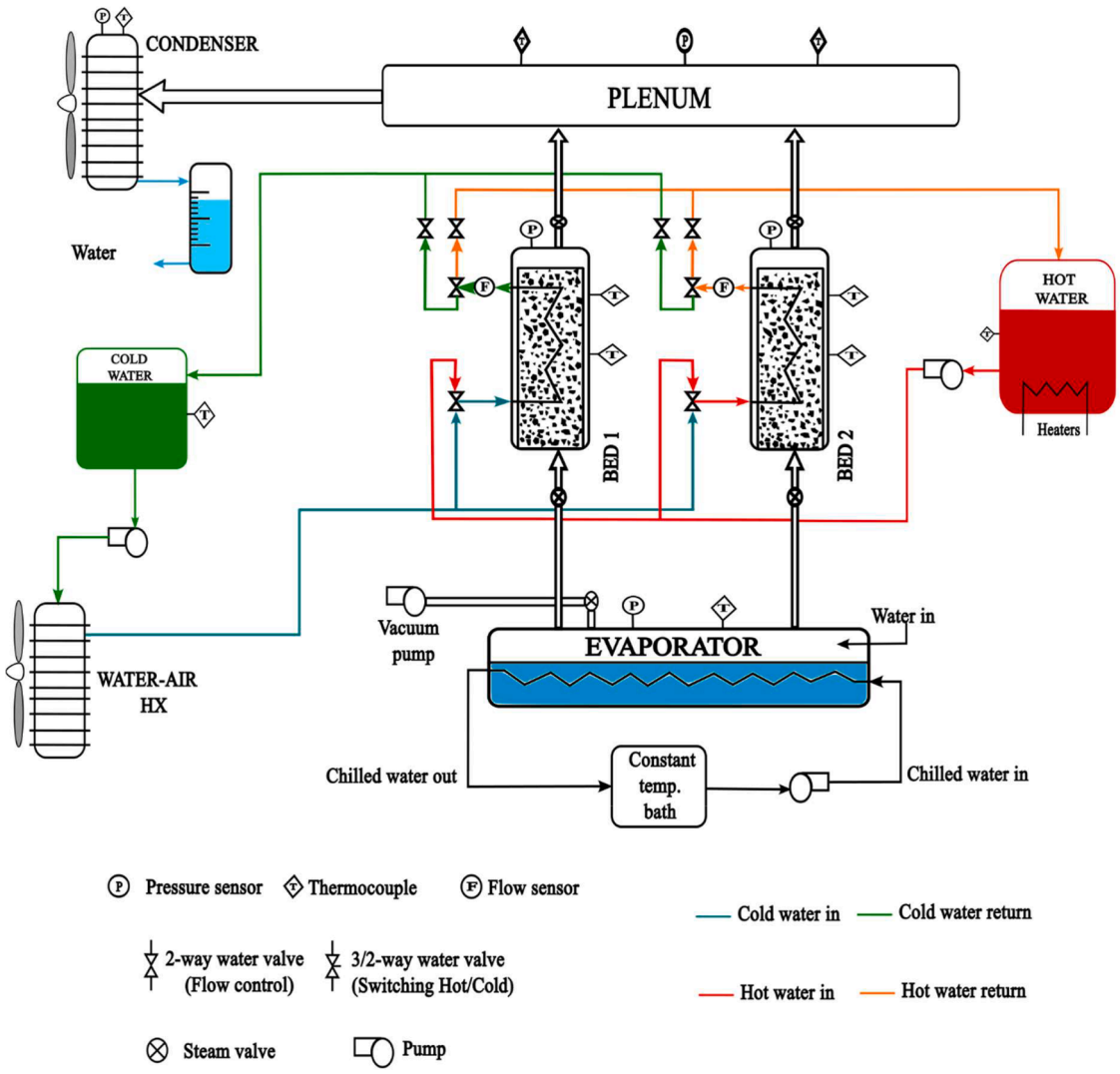

Fig. 11. Schematic of the two-bed single-stage adsorption cooling system.

implies that beyond Y_{cr}, the adsorbed bed suffers from deprivation of vapor flow which drastically reduces its performance. For a given adsorption time scale, the Y_{cr} is calculated using the following equation (Mitra et al., 2016) and its values for the three cases studied are shown in Table 3:

$$Y_{cr} = \left[\frac{p_{evap}\rho_{evap}h_{ads}K}{\mu\lambda_{bed}\Delta T}\right]^{0.5} X \tag{5}$$

where X is the thermal diffusion length (length over which thermal diffusion is dominant instead of heat of adsorption) measured from the surface of the heat exchanger tubes, p_{evap} is the evaporator pressure, ρ_{evap} is density at evaporator, μ is dynamic viscosity of vapor, h_{ads} is the heat of adsorption, K and λ_{bed} are the permeability and thermal conductivity of the adsorber bed respectively. ΔT is the difference in the temperature of the adsorber bed at the start of adsorption and temperature at which the heat transfer fluid carries away the heat of adsorption. For the present case, the following values are used in the calculation of Y_{cr} : p_{evap} =1.4 kPa, $\rho_{evap} = 7.04 * 10^{-3}$ kg m^{-3}, $\mu = 2.1 \times 10^{-5}$ Pa.s, $h_{ads} = 2690$ kJ/kg, and $\Delta T = 10$ °C. The thermal diffusion length scales are taken from the adsorber bed configuration shown in Fig. 12. The heat transfer tube geometry with 20 mm tube pitch results in variable thermal diffusion length scales i.e., 5 mm (X_1) at the sides and 9 mm (X_2) diagonally and hence two critical flow length scales (Y_{cr1} and Y_{cr2}).

For the experimental adsorber bed shown in Fig.12, the vapor passage length (Y) is 75 mm (radius of the metal mesh). A comparison between cases i and ii (Table 2) is made first. In the RD 2060 specimen (case i), the critical vapor penetration depth (Y_{cr1} and Y_{cr2} shown in Table 3) is much greater than the vapor passage length implying the vapor is available along the entire length of the adsorber bed during adsorption. This implies low flow resistance within the adsorber bed. It is the intra-particle mass diffusion resistance which determines the uptake capacity in this case. RD 3070 specimen exhibits better uptake, if same thermo-physical properties as of RD 2060 are assumed (case ii), despite the critical penetration depth (Y_{cr1} and Y_{cr2}) being less than the vapor passage length. In this case, the adsorption kinetics is dominant over inter-particle flow resistance and yields better uptake capacity. In the third case, for RD 3070, the critical vapor penetration depth (Y_{cr1} and Y_{cr2}) further decreases because of reduction in permeability. In spite of the difference in the critical vapor penetration depth values between cases ii and iii not being very significant, the uptake capacity differs

Table 3
Critical vapor flow length scales.

Case	R_p (mm)	X_1 (mm)	X_2 (mm)	Y_{cr1} (mm)	Y_{cr2} (mm)
i	0.8	5	9	103	186
ii	0.23	5	9	30	54
iii	0.23	5	9	23	42

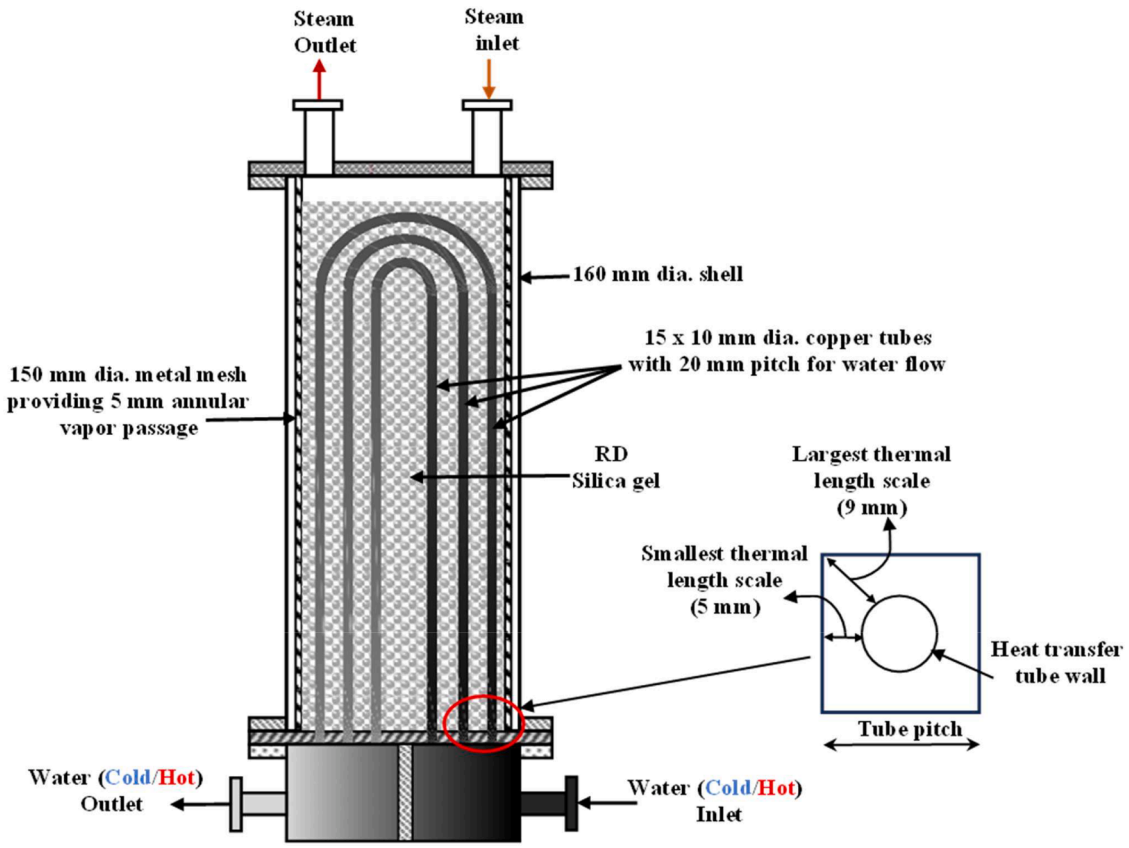

Fig. 12. Schematic of adsorber bed.

considerably.

The above deductions can be construed to influence the system level performance in all the three domains namely- adsorption kinetics, flow resistance (permeability), and thermal transience. Among them, thermal transience is the most significant one affecting the overall bed performance (Madhuri et al., 2023). *Prima facie,* when the only difference is the particle size (i.e., shape and rest of other transport properties remaining same - case ii), the adsorption kinetics is dominant over the flow and thermal kinetics resulting in the better performance by smaller sized spherical particles. However, for case iii, when the actual properties corresponding to smaller non-spherical widely distributed particle sizes are involved, only the adsorption kinetics is favorable. The increase in the other two resistances related to thermal and flow, which depend on the thermal diffusivity and permeability of the adsorber bed, substantially deteriorates its performance. Thermal diffusivity depends on the packing density and the thermal properties of the silica gel. The thermal diffusivity of RD 3070 silica gel, listed in Table 2 is 30% less than that of RD 2060. Also, it can be seen from Table 2, due to the dense packing of the adsorber bed in the case of RD 3070 (case iii), the bed porosity and, in turn, bed permeability is significantly lower than that of RD 2060. The reduced thermal diffusivity and permeability of the bed because of the non-spherical shape and non-uniform size of the silica gel results in the observed reduction in the uptake capacity despite better adsorption kinetics.

5.2. Experimental findings

The system is operated in single-stage one-bed mode at an evaporator pressure of 1.7 kPa, switching time of 450 s, half cycle time of 2700s, and heat source temperature of 85 °C. In either case, the cooling system performance is evaluated only after the system attains cyclic steady state (6 cycles).

5.2.1. Steady-state bed temperature

Fig. 13 illustrates the difference in the average bed temperature between RD 2060 and RD 3070 silica gel specimens for one thermal compression cycle. These measurements are with two thermocouples stationed at different axial locations in the adsorber bed. It can be inferred from Fig. 13 that the temperature wave form of the RD 3070 adsorber bed is significantly different from that of RD 2060. One of the reasons that can be attributed to this variance is the difference in their thermal diffusivities as seen in Table 2. The variance in the thermal

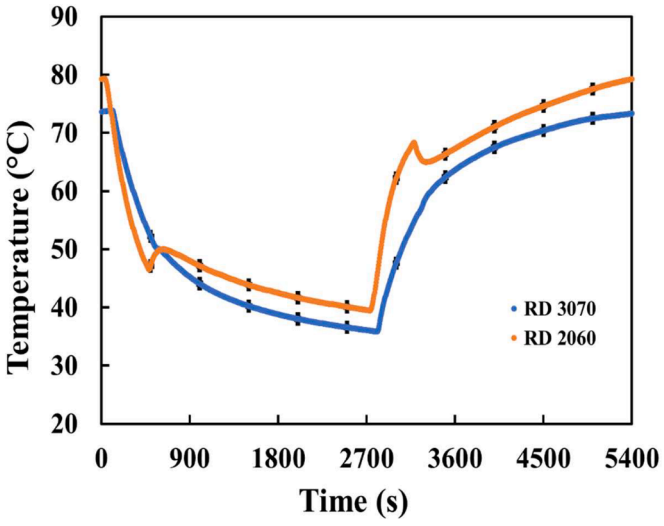

Fig. 13. Comparison of the adsorber bed average temperature between RD 2060 and RD 3070 silica gel specimens for one thermal compression cycle. Black coloured vertical lines represent error bars.

performance of both specimens is further exemplified in Fig. 14. TC1 and TC2 are located at the top and bottom of each bed along the axis and the vapor adsorption and desorption are at the top.

Fig 14a) shows that the adsorber bed is isothermal when filled with RD 2060. On the other hand, the adsorber bed with RD 3070 shows highly non-uniform axial temperature distribution (Fig. 14b)). This can be attributed to the following factors:

i) In the case of RD 2060 which has uniform spherical particles, the bed packing density remains constant and is not affected significantly during pressure cycling (adsorption and desorption) in the adsorber bed. It implies that the bed porosity and permeability remain uniform in the adsorber bed throughout the adsorption cycle. Consequently, the thermal diffusivity also can be assumed to be the same throughout the adsorber bed.
ii) With non-spherical and non-uniform, irregular particles of RD 3070, the packing density increases abating the porosity and hence permeability. In the case of spheres, the inter particle spacing cannot be decreased beyond a certain value. But for powder like non-spherical particles with wide range of size and shape distribution, the bed packing density can differ from that at the time of initial filling into the adsorber bed.
iii) Also, the pressure cycling significantly alters the adsorbent packing redistributing the adsorbent within the bed. This results in a variable axial and radial permeability and thermal diffusivity which is highly complex to estimate quantitatively.
iv) Radial distribution of thermal properties and particle distributions cannot be precluded which could also affect the bed performance.

In the case of RD 2060, because of uniform and high permeability, the entire adsorbent conglomerate interacts with vapor during adsorption and desorption. Consequently, it can be expected that the release of heat of adsorption will be synchronous over the entire volume. In tandem with uniform thermal diffusivity, congruent temperature distribution is observed at the top and bottom of the adsorber bed (Fig. 14a)). On the contrary, in Fig. 14b), the time-temperature history at the top of the bed shows slower bed cooling/heating during both sorption processes. This is due to fact that the top of the adsorber bed receives vapor flow sooner and releases heat of adsorption faster and hence the cooling rate is slower during adsorption and *vice versa* during desorption. But at the bottom of the bed, the adsorbent might be receiving negligible vapor flow, or even completely deprived of vapor flow within the cycle time allocated. Only sensible cooling/heating of the bed takes place which is clearly visible as indicated in Fig. 14b). This confirms volumetrically asynchronous ad/desorption within the adsorber bed and an imbalance in the performance of the bed during ad/desorption. The net result is a lower throughput of the cooling system. The under/non-performing adsorbent acts merely as dead mass undergoing thermal cycling alone leading to a decline in overall performance of the cooling system in comparison with RD 2060.

5.2.2. *Steady-state bed pressure dynamics*

Fig. 15 shows the time-pressure history comparison of RD 2060 and RD 3070 adsorbents where it is evident that the pressure transience is relatively much faster than the thermal transience. The switching time of 450 s is sufficient for RD 2060 as the pressure drop/rise is much lower/higher than the evaporator/condenser pressure. For RD 3070, 450 s of switching is just adequate to reach a pressure slightly lower than the evaporator pressure at the end of precooling and *vice versa* at the end of preheating. As the same mass of adsorbent is used in both the cases, in the case of RD 3070, dense packing of the adsorbent results in a higher void volume above the silica gel. It is analogous to a positive displacement compressor with a large clearance volume and slows down the rate at which pressure builds during preheating. Further, the rate of pressure build-up/decline $|dp/dt|$ is steeper for RD 2060 than for RD 3070 which can be attributed to faster sorption in the former at bed level. Slower rate in the case of RD 3070 can also be due to a larger void volume.

5.2.3. *Overall comparison of the performance of RD 2060 and RD 3070*

Typically, cooling systems are evaluated based on the temperature at

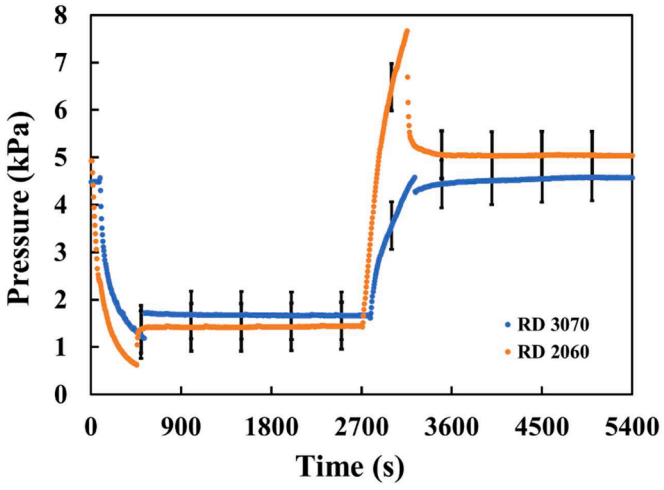

Fig. 15. Comparison of the adsorber bed pressure dynamics between RD 2060 and RD 3070 in a thermal compression cycle. Black coloured vertical lines represent error bars.

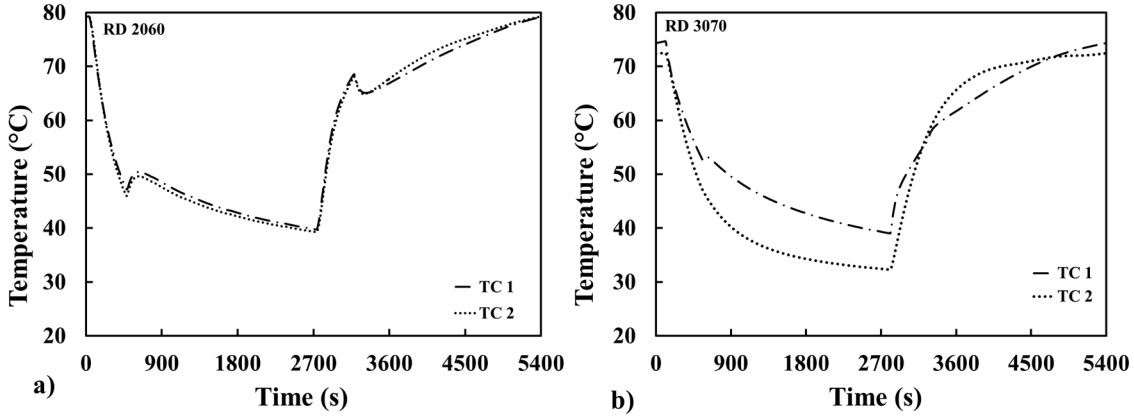

Fig. 14. Cyclic steady state time-temperature history: a) RD 2060 and b) RD 3070. TC 1 corresponds to the thermocouple located nearer to the bed inlet. TC 2 corresponds to a thermocouple located at a depth of 330 mm from the top.

which the refrigeration is obtained, CC and the COP. Fig. 16 shows the time-temperature history of evaporator in both cases.

Recalling that the adsorbers were operated in a single bed mode, the case of RD 2060 shows a systematic cycling as against RD 3070 which shows a steady evaporator temperature. The cycling in the former arises due to interconnection of the adsorber and the evaporator or absence of it. When it is exposed to the evaporator, the cooling effect is more significant than when it is disconnected from the evaporator. The temperature rise shows a first order behavior due to thermal capacitance of the evaporator. On the other hand, such a cycling is not visible for RD 3070 because of a drastic reduction in the throughput of the adsorber due to combined effect of inferior thermal properties and increased flow resistance arising from decline in porosity and permeability.

Table 4 summarizes the overall performance comparison of RD 2060 and RD 3070. The CC per cycle is calculated from the amount of condensate collected and latent heat at the evaporator condition. The difference in readings for 3 cycles is used to obtain the average condensate which results in an uncertainty of about ± 1.0%. The heat input for thermal compression per cycle is determined from the electrical heater cycling data. The COP is defined as the ratio of cooling capacity to the heat input. The calculation procedure for CC and COP is same as described in (Madhuri et al., 2023). Kline Mclinctok (Holman, n. d) method based on the root of the sum squares of the product of partial derivative of each independent variable (temperature and mass of condensate collected) and error associated in measuring it is employed for measuring the uncertainty in estimated values of CC and COP. Taking into account the error in measuring the condensate, accuracy of thermocouples, the uncertainty in CC and COP calculation are ± 1.47% and ± 3% respectively for the operating condition studied.

From the above table, it is evident that RD 3070 when used in the same cycle configuration yielded only 20% of the CC and a decline of 73% in the COP of RD 2060. This is in total contrast to report of (Vodianitskaia et al., 2017) where the decline in the COP was only 4% for a smaller particle size of 0.26 mm diameter compared to 2.0 mm diameter particles. The difference in performance can be attributed to:

i) heat rejection mode i.e., air-cooled/ water-cooled heat rejection.
ii) packed bed large sized adsorbers with multiple heat exchanger tubes.
iii) compounding of non-idealities over each cycle till the cyclic steady-state operation is attained.

5.2.4. Comparison of Dühring plots

Fig. 17 compares the Dühring plots for RD 2060 and RD 3070 specimens. The inclined lines in the Dühring plot represent isosteres (constant uptake ($kg.kg^{-1}$)). All the above-mentioned factors cause the RD 3070 adsorber bed to operate across a lower uptake differential than the RD 2060. The difference in the bed temperature and pressure dynamics in Figs. 13 and 15 is also reflected in the Dühring plot. The CC obtained using RD 3070 at the given operating conditions is always less than that obtained with RD 2060 and is about one fifth of the cooling capacity of RD 2060. This is much lower than the value anticipated from the simulation studies. In simulation studies, even though actual properties are used for RD 3070, constant values of permeability and thermal diffusivity are still used which is not true for an actual adsorber bed. Therefore, the current adsorber bed configuration is not suitable for working with smaller non-uniformly sized particles which are non-spherical. The effect of maldistribution of water vapor intake into the adsorber could also have a significant effect (Liu et al., 2014) which could have more pronounced effect on RD 3070 because of poor permeability in both axial and radial directions. Another attribute to poorer performance of RD 3070 could be due to cyclic difference between the amount adsorbed and desorbed (Gadalla, 2007). This cyclic difference could be because of the variance in the adsorbent particle size and shape dependant thermal, pressure, and mass transfer kinetics. Fig. 16 clearly indicates the variation in this cyclic difference between RD 2060 and RD 3070.

Although, at particle level a smaller size might have better adsorption characteristics, this is not replicated at the bed level when innumerable particles are packed in it. It may be inferred that the bed design must account for particle size and shape as well. In addition, the operational parameters such as switching time, half-cycle time, and heat source temperature must be chosen to be compatible with the particle size and shape. A possibility is to increase the half-cycle time to utilize the entire capacity of bed to ad/desorb the water vapor. This may lead to cycle times of the order of several hours which are impractical. To enhance the performance of the adsorber bed, it may be advisable to adopt a shallow configuration of large diameter and small height.

Table 4
Performance comparison of RD 2060 and RD 3070.

Parameter	RD 2060	RD 3070
Condensate collection duration (s)	5400	12,181
Amount of condensate collected (kg)	0.24	0.11
Cooling capacity (at ~16 °C evaporator temperature) (W)	107	22
Heat input (W)	957	890
COP	0.11	0.03

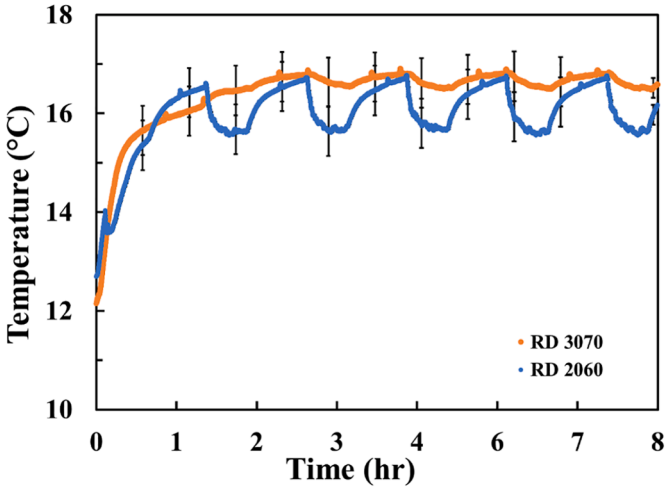

Fig. 16. Time-temperature history of evaporator for RD 2060 and RD 3070. Black coloured vertical lines represent error bars.

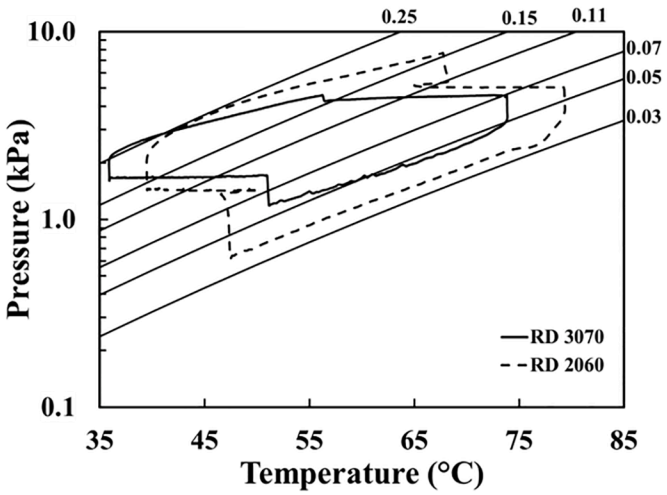

Fig. 17. Comparison of Dühring plots for RD 2060 and RD 3070.

6. Conclusions

A comprehensive comparison has been made between performance of silica gel particles of 0.8 mm (RD 2060) and 0.23 mm radius (RD 3070) in an adsorption cooling system. The initial CFD studies assuming spherical particles of different sizes showed that smaller sized spherical particles (0.23 mm) possess better adsorption characteristics than bigger sized (0.8 mm) ones. This gave impetus to experimentally investigate the performance of the cooling system with different adsorbent particle sizes. The following conclusions can be drawn from the analysis of the experimental data:

i) The steady state thermal transience within the adsorber bed is significantly different between beds packed with 0.8 mm radius and 0.23 mm nominal radius.
ii) Adsorber bed packed with 0.23 mm exhibits non-isothermal temperature distribution axially whereas the one filled with 0.8 mm shows a fairly uniform axial temperature distribution.
iii) The steady state pressure-time history confirms that pressure transience is faster than the thermal transience.
iv) In contrast to the CFD studies, 0.23 mm particle packed bed system performed poorly. Under the same operating conditions, CC obtained using 0.23 mm is only 20% of that obtained with 0.8 mm. This is attributed, inter alia, lower permeability and thermal diffusivity of the 0.23 mm radius particles arising from its non-spherical shape and non-uniform size.
v) Through this work, it is illustrated that there should be a congruence in the choice of adsorber shell orientation depending on adsorbent particle shape, size, and distribution in tandem with operational parameters, namely- half-cycle time, switching time, and heat source temperature.

CRediT authorship contribution statement

Reddy Madhuri Manila: Formal analysis, Investigation, Methodology, Validation, Writing – original draft, Writing – review & editing. **Kandadai Srinivasan:** Conceptualization, Investigation, Methodology, Supervision, Visualization, Writing – review & editing. **Pradip Dutta:** Conceptualization, Investigation, Supervision, Methodology, Writing – review & editing.

Declaration of competing interests

The authors declare that they have no known competing financial interests or personal relationships that could have appeared to influence the work reported in this paper.

Acknowledgments

The authors would like to thank the Department of Science and Technology (DST), Government of India, for the financial support for this work. Additionally, P.D. acknowledges the support of J. C. Bose Fellowship (SERB Grant No. JBR/2021/000035/SSC) and J. R. D. TATA Chair Professorship of IISc for carrying out this work.

References

Sen Chang, K., Chen, M.T., Chung, T.W., 2005. Effects of the thickness and particle size of silica gel on the heat and mass transfer performance of a silica gel-coated bed for air-conditioning adsorption systems. Appl. Therm. Eng. 25, 2330–2340. https://doi.org/10.1016/j.applthermaleng.2004.12.020.

Glaznev, I.S., Aristov, Y.I., 2010. The effect of cycle boundary conditions and adsorbent grain size on the water sorption dynamics in adsorption chillers. Int. J. Heat. Mass Transf. 53, 1893–1898. https://doi.org/10.1016/j.ijheatmasstransfer.2009.12.069.

Aristov, Y.I., Glaznev, I.S., Girnik, I.S., 2012. Optimization of adsorption dynamics in adsorptive chillers: loose grains configuration. Energy 46, 484–492. https://doi.org/10.1016/j.energy.2012.08.001.

Aristov, Y.I., 2013. Experimental and numerical study of adsorptive chiller dynamics: loose grains configuration. Appl. Therm. Eng. 61, 841–847. https://doi.org/10.1016/j.applthermaleng.2013.04.051.

Vodianitskaia, P.J., Soares, J.J., Melo, H., Gurgel, J.M., 2017. Experimental chiller with silica gel: adsorption kinetics analysis and performance evaluation. Energy Convers. Manage 132, 172–179. https://doi.org/10.1016/j.enconman.2016.11.028.

Niazmand, H., Talebian, H., Mahdavikhah, M., 2013. Effects of particle diameter on performance improvement of adsorption systems. Appl. Therm. Eng. 59, 243–252. https://doi.org/10.1016/j.applthermaleng.2013.05.043.

Chakraborty, A., Saha, B.B., Aristov, Y.I., 2014. Dynamic behaviors of adsorption chiller: effects of the silica gel grain size and layers. Energy 78, 304–312. https://doi.org/10.1016/j.energy.2014.10.015.

Mitra, S., Muttakin, M., Thu, K., Saha, B.B., 2018. Study on the influence of adsorbent particle size and heat exchanger aspect ratio on dynamic adsorption characteristics. Appl. Therm. Eng. 133, 764–773. https://doi.org/10.1016/j.applthermaleng.2018.01.015.

Manila, M.R., Mitra, S., Dutta, P., 2020. Studies on dynamics of two-stage air cooled water/silica gel adsorption system. Appl. Therm. Eng. 178, 115552 https://doi.org/10.1016/j.applthermaleng.2020.115552.

Mahdavikhah, M., Khatibi, M., Niazmand, H., 2019. Relative importance of inter-particle mass transfer resistance in the modeling of adsorption chiller porous bed. Int. J. Refrig. 106, 104–112. https://doi.org/10.1016/j.ijrefrig.2019.06.005.

AKISAWA, A., TAMOGAMI, A., TAKEDA, N., NAKAYAMA, M., NATSUI, T., 2022. Effect of adsorbent on the performance of double effect adsorption refrigeration cycle with adsorption heat recovery. Int. J. Refrig. 141, 21–30. https://doi.org/10.1016/j.ijrefrig.2022.06.012.

Sircar, S., Hufton, J.R., 2000. Why does the linear driving force model for adsorption kinetics work? Adsorption 6, 137–147. https://doi.org/10.1023/A:1008965317983.

El-Sharkawy, I.I., 2011. On the linear driving force approximation for adsorption cooling applications. Int. J. Refrig. 34, 667–673. https://doi.org/10.1016/j.ijrefrig.2010.12.006.

Kaviany, M., 1999. Principles of Heat Transfer in Porous Media, 2nd ed. Springer.

Carman, P.C., 1956. Flow of Gases Through Porous Media. Butterworths Scientific Publications.

Mitra, S., Aswin, N., Dutta, P., 2016. Scaling analysis and numerical studies on water vapour adsorption in a columnar porous silica gel bed. Int. J. Heat. Mass Transf. 95, 853–864. https://doi.org/10.1016/j.ijheatmasstransfer.2015.12.011.

Madhuri, M.R., Srinivasan, K., Dutta, P., 2023. Performance evaluation of a two-stage air-cooled silica gel + water adsorption cooling system : effect of key operational parameters. Appl. Therm. Eng., 120991 https://doi.org/10.1016/j.applthermaleng.2023.120991.

J.P. Holman, Eighth Edition, n.d.

Liu, Y., Zheng, X., Dai, R., 2014. Numerical study of flow maldistribution and depressurization strategies in a small-scale axial adsorber. Adsorption 20, 757–768. https://doi.org/10.1007/s10450-014-9619-7.

Gadalla, M.A., 2007. Simulation of intermittent thermal compression processes using adsorption technology. J. Franklin. Inst. 344, 725–740. https://doi.org/10.1016/j.jfranklin.2005.12.007.